Computers in Biology and Medicine 111 (2019) 103355

Contents lists available at ScienceDirect

Computers in Biology and Medicine

journal homepage: www.elsevier.com/locate/compbiomed

Prediction of epileptic seizures with convolutional neural networks and functional near-infrared spectroscopy signals

Roberto Rosas-Romero[a,*], Edgar Guevara[b], Ke Peng[c], Dang Khoa Nguyen[d], Frédéric Lesage[c,e], Philippe Pouliot[c,e], Wassim-Enrique Lima-Saad[a]

[a] Universidad de las Américas-Puebla, Mexico
[b] CONACYT - Universidad Autónoma de San Luis Potosí, Mexico
[c] École Polytechnique de Montréal, Canada
[d] Hôpital Notre-Dame du CHUM, Canada
[e] Montreal Heart Institute, Canada

ARTICLE INFO

Keywords:
Convolutional neural network (CNN)
Epileptic seizure prediction
Functional near-infrared spectroscopy (fNIRS)
Gradient descent method

ABSTRACT

There have been different efforts to predict epileptic seizures and most of them are based on the analysis of electroencephalography (EEG) signals; however, recent publications have suggested that functional Near-Infrared Spectroscopy (fNIRS), a relatively new technique, could be used to predict seizures. The objectives of this research are to show that the application of fNIRS to epileptic seizure detection yields results that are superior to those based on EEG and to demonstrate that the application of deep learning to this problem is suitable given the nature of fNIRS recordings. A Convolutional Neural Network (CNN) is applied to the prediction of epileptic seizures from fNIRS signals, an optical modality for recording brain waves. The implementation of the proposed method is presented in this work. Application of CNN to fNIRS recordings showed an accuracy ranging between 96.9% and 100%, sensitivity between 95.24% and 100%, specificity between 98.57% and 100%, a positive predictive value between 98.52% and 100%, and a negative predictive value between 95.39% and 100%. The most important aspect of this research is the combination of fNIRS signals with the particular CNN algorithm. The fNIRS modality has not been used in epileptic seizure prediction. A CNN is suitable for this application because fNIRS recordings are high dimensional data and they can be modeled as three-dimensional tensors for classification.

1. Introduction

Prediction of epileptic seizures refers to the analysis of brain signals, extracted from an epileptic patient, to detect the future occurrence of a seizure. There are four states within a brain signal, which is extracted from an epileptic patient. The *ictal* state is the signal fragment where an epileptic seizure occurs; the *pre-ictal* state is the segment that happens before the onset of a seizure; *post-ictal* is the state that follows a seizure, and *inter-ictal* is the fragment between the end of post-ictal and the start of pre-ictal. In this work, we merge post-ictal and inter-ictal states into one state, inter-ictal. Furthermore, we discard the ictal state since detecting an epileptic seizure, when it is happening, is of no interest for seizure prediction. Thus, we only consider two states, inter-ictal and pre-ictal. Epileptic seizure prediction is achieved when the system detects the pre-ictal state [1].Real-time epileptic seizure prediction mainly consists of two stages: (1) extraction of a tensor from the signal of interest, at any time position; and (2) classification of the tensor as inter-ictal or pre-ictal. Epileptic seizures are predicted when pre-ictal segments are correctly detected. Detection of the ictal state is of no interest since the goal is detecting a seizure before it happens by identifying the occurrence of the pre-ictal state. Thus, ictal fragments are of no use. There have been different efforts to predict seizures and most of them are based on the analysis of *electroencephalography* (EEG) signals [2]; however, recent publications have suggested that fNIRS signals, a relatively new modality, could be used to predict seizures [3,4]. fNIRS (*functional near-infrared spectroscopy*) is an optical technique, which conveys monitoring information about brain activity [5]; specifically, two physiological parameters or measurements, the relative level of *oxygenated hemoglobin* (HbO) and the relative level of *deoxygenated hemoglobin* (HbR). fNIRS signals are generated by injecting infrared lights of different wavelengths (650 nm–1000 nm) into the scalp, followed by registration of reflected light through optodes. Blood

* Corresponding author.
E-mail address: roberto.rosas@udlap.mx (R. Rosas-Romero).

https://doi.org/10.1016/j.compbiomed.2019.103355
Received 7 May 2019; Received in revised form 8 July 2019; Accepted 8 July 2019

hemoglobin has different levels of light absorption and reflection depending on the level of blood oxygen due to brain activity [5,6]. fNIRS recordings arise from multiple channels. At each channel, two values are registered, HbO and HbR.fNIRS is a non-invasive neuroimaging technique that is effective for the monitoring of cortical hemodynamic changes. Studies have shown that fNIRS can be used to assess cortical hemodynamic changes associated with seizures, helping in the detection of seizures and the assessment of their impact on brain oxygenation [4]. Optical sensors (such as ratiometric nano quantum dot fluorescence resonance energy transfer sensors) were used to quantitatively measure oxygen dynamics from single-cell microdomains during oxygen-deprivation episodes (hypoxic episodes) and during induced seizure-like events in rats. A substantial decrease in the oxygenation of pyramidal cells was found through the concomitant measurement of blood oxygenation and electrical neural activity. This decrease in oxygen levels took place up to a few seconds before ictal activity could be revealed in electrophysiological recordings. Hence, an internally generated deficiency in oxygen is a crucial and decisive factor for hemodynamics related to epileptiform patterns [7]. The use of fNIRS in seizure prediction is based on scientific evidence that BOLD (Blood oxygen-level dependent) activity may result from neuronal changes occurring several seconds before a surface EEG event [8], and that vasoconstriction of blood vessels occurs a few seconds before the electrical onset [9]. A suitable format for fNIRS data consists of a two- or three-dimensional grid, which is the result of recording signals from multiple channels (rows), at multiple time positions (columns), by using two different measured values (feature maps or planes), HbO and HbR. Motivations for applying *Convolutional Neural Networks* (CNNs) to the problem of predicting epileptic seizures are (1) a large number of fNIRS channels, (2) the three-dimensional grid topology of fNIRS data, and (3) the straight application of raw fNIRS data to a CNN, where appropriate features are progressively extracted at convolutional layers for further classification. The use of fNIRS recordings for automated epileptic seizure detection requires more explorative studies. There are not public datasets related to fNIRS recordings on epileptic patients. This work is one of the firsts where fNIRS and deep learning are used to tackle the problem of seizure prediction. Detection of epileptic seizures in advance would allow epileptic patients or their caretakers to take precautions before the occurrence of an epileptic seizure, therefore mitigating risks and potential harm associated with the event, for instance in the intensive care unit, where electroencephalography (EEG) is typically not monitored. This document is organized as follows: Section 2 presents previous work. Section 3 provides the Convolutional Neural Network framework for the classification of fNIRS tensors, which includes a description of the architecture parameters and the implementation of the learning algorithm. Section 4 gives details of the methodology followed in this research. The results of this work are presented in Section 5 and discussed in Section 6. Finally, conclusions are given in Section 7.

2. Related work

Predicting epileptic seizures is the core of monitoring and warning systems so that precautions are taken before a seizure occurs [2]. One of the main problems for patients with epilepsy is the unpredictability of seizures [10]. Seizure detection and prediction have been mostly based on EEG recordings [1,2,11–15] given its capability to monitor electrical activity from the brain at a high temporal resolution [16]. EEG is the fastest and cheapest non-invasive method for monitoring of brain electrical activity. Nonetheless, EEG modality presents some disadvantages such as low spatial resolution [17], registration of changes when neurons in a large area of cortex synchronize [18], propagation of electrical currents along with the extracellular spaces [18], background noise and motion artifacts such as eye movement and muscle activity [12]. Feature extraction techniques, which have been applied to EEG signals, are frequency analysis, time analysis, wavelet analysis, entropy measurements, principal component analysis, and empirical mode decomposition. Some techniques, used to classify EEG signals, are Artificial Neural Networks, Support Vector Machines, Decision Trees and Gaussian Mixture Models. In this work, fNIRS is applied to predict seizures. One motivation for the selection of this modality is that it has been successfully used in the long-duration monitoring of epileptic patients [5,16], the analysis of hemodynamics in epilepsy [6], identification of ictal onset for pre-surgical evaluation [19], and the study of neurological diseases [5]. fNIRS signals present advantages [16], they reflect changes in local blood volume; recording of these signals does not require immobilization, and they present high temporal resolution. Nonetheless, this modality has its disadvantages [16], such as low spatial resolution; sensitivity to certain movements, which might introduce artifacts; and hair represents a problem for its implementation. In general, fNIRS and EEG technologies are robust against motion artifacts, do not require subject immobilization as other modalities, the cost for their hardware implementation is lower than that of other modalities, and do not involve exposure to high radiations. Synchronous extraction of fNIRS and EEG is also getting increased interest because of the absence of electro-optical interference, and the simple integration of both noninvasive recordings. There have been efforts where fNIRS and EEG are combined during acquisition without major discomforts in patients [20]. Within clinical applications, different areas have used fNIRS-EEG integration [21]: newborn (37%), epilepsy (27%), surgery (16%), rehabilitation (8%), child development (6%), and psychiatry (6%). Integrated synchronous measurements of EEG and fNIRS have been performed on epileptic patients [16,22] to assess the usefulness of fNIRS in epileptic patients focused on the hemodynamic mechanisms before, during, and after seizures at different time scales and brain locations [23]. There is an analysis to improve the detection of epileptic activity using fNIRS, which gives a comparison of time-domain with time-frequency domain (wavelet) methods based on the general linear model approach to detect hemodynamic responses during epileptic activity [24]. Other studies involving EEG and fNIRS measurements were directed towards epileptogenic focus localization [19,25]. We have applied the fNIRS-EEG integration to the prediction of refractory epilepsy, which provides an enhanced performance when compared with a prediction based on EEG recordings alone [26]; however, seizure prediction based on fNIRS alone showed the same performance as a prediction based on the fNIRS-EEG integration [26]. Thus, we are focusing on using fNIRS alone with the advantage of a reduced number of total channels without compromising the performance of the classifier. Even though fNIRS recordings have been used to study different aspects of epilepsy [15], fNIRS recordings have not yet been completely studied as a tool for seizure prediction [26].

3. Implementation of a convolutional neural network

This section provides the framework for the complete implementation of a convolutional neural network (CNN) along with the corresponding learning algorithm. This section introduces the notation that is used to describe the selection of the most appropriate CNN model for seizure prediction. This notation is later used in the Results section, which shows the outcome of a set of experiments aimed at selecting the CNN model parameter values.

3.1. Architecture

A convolutional neural network (CNN) is a learning machine, which broadly consists of two stages, a feature extraction stage based on convolutional layers, and a subsequent classification stage based on classification layers. The format of fNIRS data fed to a CNN is a three-dimensional tensor $\mathbf{x} \in \mathbf{R}^{W \times H \times D}$. At a convolutional layer, neural nodes are arranged in a three-dimensional grid. A neural node, within a convolutional layer, is connected to a subset of nodes from a previous convolutional layer (local connectivity) through *kernel coefficients*. At a

convolutional layer, each node processes information through three operations: *convolution*, followed by an *activation function*, followed by a *pooling* operation. All neural nodes, in a convolutional layer, share the same set of kernel coefficients for the incoming signals to the node (parameter sharing).

3.2. Feedforward propagation

A convolutional layer ℓ is fed with a 3-D data tensor $\mathbf{y}^{\ell-1}=\left\{y^{l-1}_{i,j,k};\ 1\le i\le W_D^{\ell-1};\ 1\le j\le H_D^{\ell-1};\ 1\le k\le D_D^{\ell-1}\right\}$, which is the output data tensor from the previous adjacent layer $\ell-1$. Indexes i, j, and k specify tensor *column*, *row*, and *plane*, respectively. Parameters $W_D^{\ell-1}$, $H_D^{\ell-1}$, $D_D^{\ell-1}$ are tensor dimensions, *width* (columns), *height* (rows), and *depth* (number of tensor planes), respectively. Fig. 1 shows the tensor flow over the three operations in a convolutional layer (convolution, activation, and pooling) along with the tensor dimensions after each operation.

At convolutional layer ℓ, a 3-D input tensor $\mathbf{y}^{\ell-1}$ is convolved with each 3-D kernel in a bank of kernels $\{\omega^{\ell,1},\omega^{\ell,2},\cdots,\omega^{\ell,D_D^\ell}\}$ to generate the 3-D tensor $\mathbf{v}^\ell=\{v^\ell_{i,j,k};\ 1\le i\le W_D^{\ell-1},\ 1\le j\le H_D^{\ell-1},\ 1\le k\le D_D^\ell,\ 1\le\ell\le L\}$, where $\mathbf{v}^\ell_p=\mathbf{y}^{\ell-1}*\omega^{\ell,p};\ 1\le p\le D_D^\ell$. The convolution of tensor $\mathbf{y}^{\ell-1}$ and kernel $\omega^{\ell,p}$ generates a *feature map* or (*plane*) $\mathbf{v}^\ell_p$. The number of planes in tensor $\mathbf{v}^\ell$ is the same as the number of kernels in the bank. Kernel dimensions are width W_K^ℓ, height H_K^ℓ, and depth D_K^ℓ. Each kernel is identified by a super-index p, $\omega^{\ell,p}=\left\{\omega^{\ell,p}_{m,n,k};\ -\frac{W_K^\ell-1}{2}\le m\le\frac{W_K^\ell-1}{2},\ -\frac{H_K^\ell-1}{2}\le n\le\frac{H_K^\ell-1}{2},\ 1\le k\le D_K^\ell,\ \text{where}\right.$

$$\left.,\ 1\le p\le D_D^\ell,\ 1\le\ell\le L\right\}$$

width W_K^ℓ and *height* H_K^ℓ are odd numbers and the kernel *depth* D_K^ℓ is the same as the depth of the input data tensor $D_D^{\ell-1}$. An entry $v^\ell_{i,j,k}$ in tensor $\mathbf{v}^\ell$ is given by

$$v^\ell_{i,j,p}=b^\ell_p+\sum_{m=-\frac{W_K^\ell-1}{2}}^{\frac{W_K^\ell-1}{2}}\sum_{n=-\frac{H_K^\ell-1}{2}}^{\frac{H_K^\ell-1}{2}}\sum_{k=1}^{D_K^\ell}\omega^{\ell,p}_{m,n,k}\,y^{\ell-1}_{i+m,j+n,k};$$
$$1\le i\le W_D^{\ell-1},\ 1\le j\le H_D^{\ell-1},\ 1\le p\le D_D^\ell,\ 1\le\ell\le L \tag{1}$$

where b^ℓ_p is the bias for kernel p at convolutional layer ℓ, and L is the number of convolutional layers. According to Fig. 1, the tensor $\mathbf{v}^\ell$ is transformed into $\mathbf{z}^\ell$ in a one-to-one correspondence through an operation, known as activation $z^\ell_{i,j,k}=f(v^\ell_{i,j,k})$. The activation function is the hyperbolic tangent function, $f(v)=\frac{e^v+e^{-v}}{e^v-e^{-v}}$. The dimensionality of the output data tensor $\mathbf{y}^\ell$ is lower than that of the input data tensor $\mathbf{y}^{\ell-1}$, and this dimensionality reduction is achieved through an operation, called *pooling*. Pooling replaces and combines multiple entries in tensor $\mathbf{z}^\ell$ into one single element in tensor $\mathbf{y}^\ell$. There are different pooling operations and the average operation is chosen since it is differentiable,

$$y^\ell_{i,j,k}=\frac{1}{r^2}\sum_{m=1}^{r}\sum_{n=1}^{r}z^\ell_{(i-1)r+m,(j-1)r+n,k};$$
$$1\le i\le W_D^\ell,\ 1\le j\le H_D^\ell,\ 1\le k\le D_D^\ell,\ 1\le\ell\le L, \tag{2}$$

where the output tensor dimensions $W_D^\ell\times H_D^\ell$ are the result of reducing the input tensor dimensions $W_D^{\ell-1}\times H_D^{\ell-1}$ by a factor $r\times r$, according to $W_D^\ell\times H_D^\ell=\frac{W_D^{\ell-1}}{r}\times\frac{H_D^{\ell-1}}{r}$. Pooling does not modify the depth dimension.

3.3. Backpropagation algorithm

A tensor propagates forward over the neural network and, after it reaches the output, the network weights are adjusted recursively and working backwards from the output convolutional layer to the input layer. The adjustment of weights is accomplished through the computation of their gradients, according to the rule

$$\omega^{\ell,p}_{i,j,k}(t+1)=\omega^{\ell,p}_{i,j,k}(t)-\eta\frac{\partial J}{\partial\omega^{\ell,p}_{i,j,k}};$$
$$1\le i\le W_K^\ell,\ 1\le j\le H_K^\ell,\ 1\le k\le D_K^\ell,\ 1\le p\le D_D^\ell,\ 1\le\ell\le L, \tag{3}$$

where $\omega^{\ell,p}_{i,j,k}(t+1)$ is a *kernel weight* at iteration $t+1$, $J(\omega^\ell)$ is the *cost function* to be minimized, $\frac{\partial J}{\partial\omega^{\ell,p}_{i,j,k}}$ is the *gradient* for adjustment of kernel weights, η is the *learning rate*, and L is the number of convolutional layers. The cost function J is the sum of all square errors $\sum_i(y_i^{L_2}-d_i)^2$, between the final network outputs and the corresponding *targets*. The computation of the kernel weight $\omega^{\ell,p}_{m,n,k}$ requires previous computation of intermediate variables, called *local gradients* $\left\{\delta^\ell_{i,j,p}=\frac{\partial J}{\partial v^\ell_{i,j,p}};\ 1\le i\le W_D^{\ell-1},\ 1\le j\le H_D^{\ell-1},\ 1\le p\le D_D^\ell\right\}$, according to

$$\frac{\partial J}{\partial\omega^{\ell,p}_{m,n,k}}=\sum_{i=1}^{W_D^{\ell-1}}\sum_{j=1}^{H_D^{\ell-1}}\delta^\ell_{i,j,p}\,y^{\ell-1}_{i+m,j+n,k};$$
$$-\frac{W_K^\ell-1}{2}\le m\le\frac{W_K^\ell-1}{2},\ -\frac{H_K^\ell-1}{2}\le n\le\frac{H_K^\ell-1}{2},\ 1\le k\le D_K^\ell,$$
$$1\le p\le D_D^\ell,\ 1\le\ell\le L. \tag{4}$$

The computation of the local gradient $\delta^\ell_{i,j,p}=\frac{\partial J}{\partial v^\ell_{i,j,p}}$, is given by

$$\delta^\ell_{(i-1)r+m,(j-1)r+n,p}=$$
$$\frac{1}{r^2}f'(v^{(i-1)r+m,(j-1)r+n,p}_{L_1})\sum_{s=-\frac{W_K^{\ell+1}-1}{2}}^{\frac{W_K^{\ell+1}-1}{2}}\sum_{t=-\frac{H_K^{\ell+1}-1}{2}}^{\frac{H_K^{\ell+1}-1}{2}}\sum_{q=1}^{D_D^{\ell+1}}\delta^{\ell+1}_{i-s,j-t,q}\,\omega^{\ell+1,q}_{s,t,p};$$
$$1\le i\le W_D^\ell,\ 1\le j\le H_D^\ell,\ 1\le m\le r,\ 1\le n\le r,\ 1\le p\le D_D^\ell$$
$$,\ 1\le\ell\le L-1, \tag{5}$$

where r is the width and height of the pooling window. The

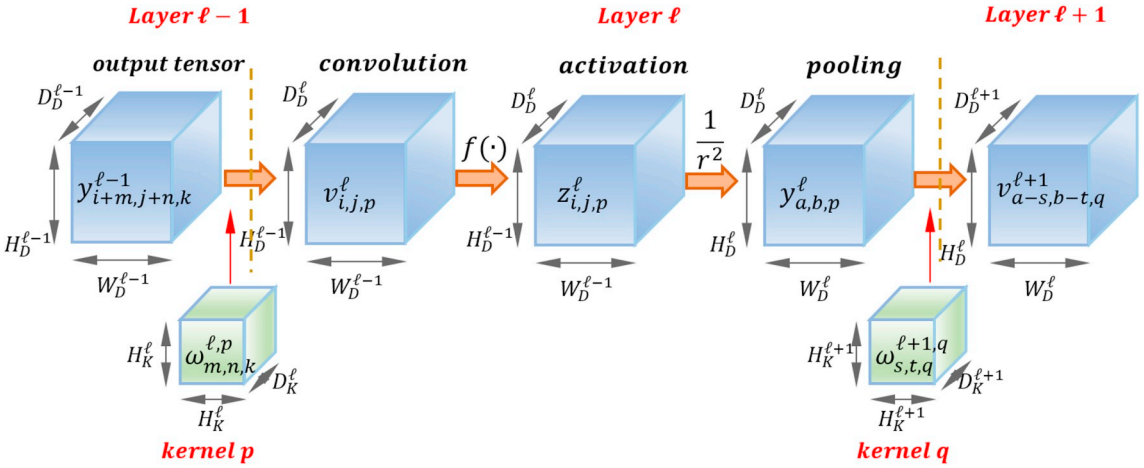

Fig. 1. Tensor flow over a convolutional layer ℓ. The input tensor is the output tensor from the previous layer ℓ - 1. Tensor dimensions are specified in detail.

computation of kernels starts at the final layer and ends with the kernels at the first convolutional layer.

4. Methods

4.1. Dataset

There are not public datasets with fNIRS recordings from patients with epileptic seizures. The dataset for this work was the result of recording fNIRS signals from patients with focal refractory epilepsy. These recordings were performed and analyzed by epileptologists from Hôpital Notre-Dame du Centre Hospitalier de l'Université de Montréal. Forty-nine patients were subjects for the generation of the dataset; however, only five patients presented epileptic seizures while recording their brain signals since an epileptic seizure is a rare event. Seizure onset, ictus and offset were determined by the epileptologist, based on clinical and electrophysiological data. This dataset has been already used for the study of inter-ictal epileptiform discharges [6,27,28]. The recording time, number of sessions and the number of channels (number of optodes) are different for each patient. Table 1 shows the information of the five patients, who showed epileptic seizures during recording sessions.

A detailed description of the EEG-fNIRS recording process can be found in Peng et al. (2014) and Nguyen et al. (2012) [27,28]. Custom helmets were designed for different head sizes and 64 light sources, up to 16 detectors, and 19 carbon EEG electrodes were mounted onto patient heads. EEG data were recorded at 500 Hz with a *Neuroscan Synamps* 2TM system (Compumedics, U. S. A.). The fNIRS data were recorded simultaneously using an optical multi-channel *Imagent Tissue Oximeter* (ISS Inc., Champaign, IL, U.S.A.). Multiple optical channels (115 ± 39 channels per subject) were used in each patient. An optical channel consisted of one source and one detector that could receive several sources. Optical channels were located 3–5 cm apart to ensure sensitivity to cortical tissue. Two wavelengths were used, one at 690 nm, which is more sensitive to HbR; and the other at 830 nm, which is more sensitive to HbO. The channel positions were arranged in an area that included the whole lobe covering the most probable epileptic focus, the contralateral lobe, and the highest possible extension of other lobes. fNIRS channels were sampled at a frequency of 19.5312 Hz. Two to twelve consecutive 15-min sessions were recorded for each patient. During the recordings, the patient was asked to sit comfortably and relax. Seizure events were marked offline, on the EEG trace of an *Analyzer 2.0* (Brain Products GmbH, Germany), by a certified neurophysiologist and reviewed by an epileptologist. HbR and HbO concentration changes were computed from light intensity using the modified Beer-Lambert Law [29].Fig. 2 shows a plot of one brain signal (HbO measurement), extracted from an epileptic patient, which includes three states: ictal (green segment), pre-ictal (red segment), and inter-ictal (blue segment). The amplitude of the signal is specified as the hemoglobin variation percentage, assuming a typical baseline of 75 μM for HbO signal and 25 μM for HbR [30]. Epileptic seizure prediction is achieved when red fragments, which correspond to pre-ictal states, are detected.

To suppress noise, coming from different sources (mainly motion artifacts), sample values greater than the mean value by three standard deviations were removed. Also, temporal filtering was applied based on a low-pass filter with an SPM8 canonical hemodynamic response function with a 4s full width at half maximum, which corresponds to 0.6 Hz cutoff frequency [31], and a fourth-order IIR high-pass filter with maximally flat response and cutoff frequency at 0.01 Hz [32] was applied.

Table 1
Information regarding patient population whose recordings integrate the dataset.

Patient	fNIRS Channels	Recording Sessions	Epileptic Seizures	Recording Time in min.
16	146	12	1	170.49
22	133	6	4	83.88
26	104	1	1	11.28
38	138	2	5	30.76
47	135	4	11	61.28

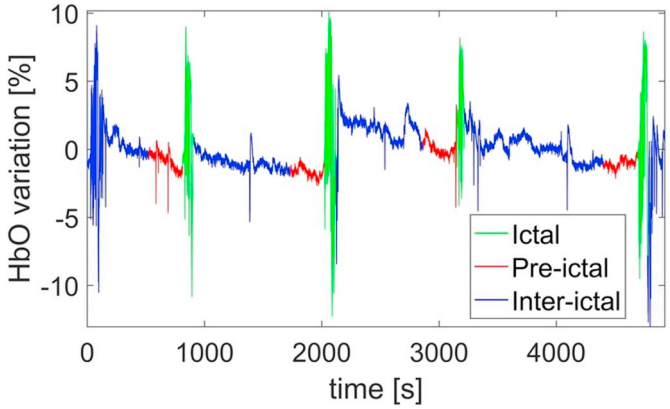

Fig. 2. Three states (ictal, inter-ictal and pre-ictal) within an HbO signal, extracted from an epileptic patient.

4.2. Synchronization and normalization of electrical and optical signals

EEG and fNIRS signals are simultaneously acquired to compare seizure prediction based on fNIRS vs. prediction based on EEG; however, they were sampled at different sampling rates. EEG signals were extracted from 19 channels at 500 Hz whereas fNIRS signals were sampled at 19.5312 Hz. This EEG-fNIRS acquisition system has been described in previous work [28]. Marks, to indicate the beginning and end of an ictal state within the ground truth for EEG channels, were established by the epileptologist. For each patient, labeling the ictal state within fNIRS channels is possible by linearly interpolating fNIRS samples so that the number of these samples matches the number of EEG samples. Interpolation of fNIRS not only allows the synchronization of fNIRS with EEG and labeling of fNIRS data but also the synthesis of fNIRS data for better evaluation of the algorithm. The signal out of each channel is normalized so that values, from different channels, lie within the same range. This normalization prevents poor classification. Each channel value, $x_i(t)$, is normalized by assigning to it a new value, $\hat{x_i}(t) = \frac{x_i(t)-\mu_i}{3\sigma i}$, where i is the channel index, μ_i is the mean value of channel i, and σ_i is the standard deviation. During real-time processing, each incoming channel value $x_i(t)$ is normalized by using these two precomputed parameters.

4.3. Tensor extraction from fNIRS signals

At each time position t, a three-dimensional tensor, $\mathbf{x}_t \in R^{H\times W\times D}$, is extracted from fNIRS channels, where dimensions H, W are D are height, width and depth, respectively. Fig. 3 shows the extraction of a tensor from fNIRS channels, where W is the number of sampled time positions, H is the number of channels, and D is the number of planes or signal modalities (HbO and HbR). A two-dimensional format is extracted from fNIRS channels when one single measurement, HbO or HbR, is used.

fNIRS values within a tensor correspond to samples taken at W time positions $\{t, t-1, t-2, \ldots, t-W+1\}$. The tensor elapsed time depends on the sampling rate for fNIRS signals and it is given by $\frac{W\ samples}{500\ Hz}$. According to Table 1, the number of channels H is different for each patient and H depends on the number of optodes on the patient scalp. Since the number of channels (tensor height) depends on each patient, a

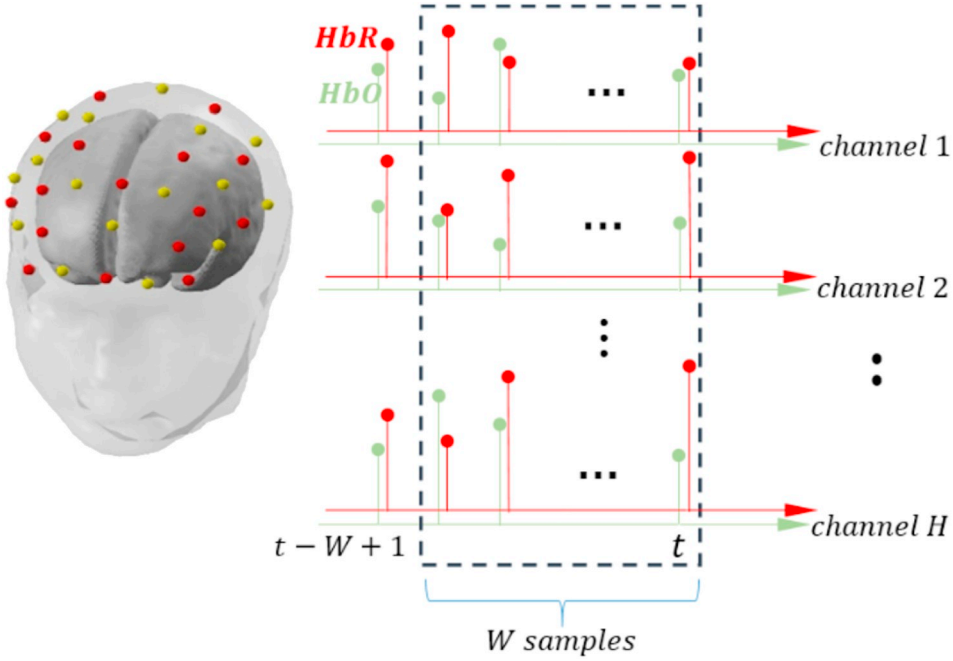

Fig. 3. Extraction of a three-dimensional tensor from a multi-channel signal at *t*. Tensor *height H* is the number of channels, *widthW* is the number of sampled time positions, *depthD* is the number of measurements (HbO and HbR).

different CNN architecture is built for each patient. Therefore, a CNN is only tested on the same patient, whose recordings were used for the training of that CNN; and it is not tested in other patients. For the case of three-dimensional tensors, depth D is two and each feature map corresponds to one reading, one for HbO and another for HbR. Two signal readings take place at each optode (one for HbO and another for HbR), and both values are assigned tensor positions with the same row and column, but at different planes. These two values are spatially correlated since they are extracted in the same position from the same optode. The tensor format is appropriate for fNIRS data since the spatial correlation of the two readings (HbO and HbR) is maintained within the tensor structure.

4.4. Labeling of tensors

A tensor is assigned one of two classes, pre-ictal or inter-ictal. Epileptologists analyzed each brain signal to mark the beginning and end of an ictal state (ground truth). In this work, it is assumed that the pre-ictal state takes place within a 5-min or 2-min window before the ictal onset. The number of pre-ictal samples within a 5-min window is $500\ \frac{samples}{second} \times 60\ \frac{seconds}{minute} \times 5\ \text{min} = 150{,}000\ samples$; while the number of pre-ictal samples within a 2-min window is 60,000 *samples*. The beginning of a pre-ictal state is determined by subtracting the number of samples within the pre-ictal window from the beginning of the ictal state. Red signal segments, in Fig. 1, correspond to pre-ictal windows. The size of the pre-ictal window is chosen arbitrarily since there is no convention on the total length of a pre-ictal state [33]. In this work, the size of the pre-ictal window depends on the recording time, the number of seizures per patient, and the proximity between consecutive seizures. For patients 38 and 47, the time length of the pre-ictal window is 2 min while patients 16, 22 and 26 are characterized by a 5-min window during pre-ictal states. A 2-min window is chosen when the ratio of recording time over the number of seizures is less than or close to 5 min. The recording time and the number of seizures in patients 38 and 48 do not allow 5-min pre-ictal segments and the corresponding 5 min of inter-ictal activity for each seizure.

4.5. Classification of tensors

The theoretical framework for convolutional neural networks is discussed in Section 3. This section provides details for CNN implementation such as the description of the parameters of a CNN architecture, tensor flowing over different convolutional and classification layers, and the CNN learning algorithm.For each patient, three different CNNs are implemented. Each CNN architecture corresponds to one possible combination of HbO and HbR measurements: HbO alone, HbR alone, and HbO + HbR. The structure of the input data tensor depends on the corresponding combination. A two-dimensional structure is required for tensors, extracted from HbO or HbR measurements; while a three-dimensional format is used for tensors arising from simultaneous readings of HbO and HbR values. For each patient and each combination of measurements (HbO, HbR), a CNN architecture is selected after training and testing separate architectures for each possible combination of parameters (model selection). The parameters to be combined are the *number of kernels* (1, 2 and 3) at each convolutional layer and the *kernel receptive fields* (3×3, 5×5 and 7×7). For each patient, the input tensor height (number of rows) is different since this parameter is the same as the *number of channels*, which were used to extract fNIRS signals during recording sessions. The second column of Table 1 shows the number of channels for each patient. For each patient, tensor dimensions are reduced at subsequent convolutional layers because of pooling.

4.6. Training and testing datasets

Tensors, extracted from a patient recording, are stored into two sets: C_1 with inter-ictal tensors, C_2 with pre-ictal tensors. Ictal tensors are not generated, since the detection of seizures while they are happening is of no interest. Some tensors, from the largest set, are discarded since C_1 and C_2 are required to have the same size so that there is no bias while the CNN learns to discriminate between both classes due to a balanced training set. Each set, C_1 and C_2, is separated into five fragments, $C_1 = \{c_{1,1}, c_{1,2}, c_{1,3}, c_{1,4}, c_{1,5}\}$ and $C_2 = \{c_{2,1}, c_{2,2}, c_{2,3}, c_{2,4}, c_{2,5}\}$. Then, a fragment $c_{1,i}$ (from C_1) and a corresponding fragment $c_{2,i}$ (from C_2) are randomly combined into c_i. The result of these random mixings is five

fragments or *folds* $\{c_1, c_2, c_3, c_4, c_5\}$, where each fragment contains pre-ictal and inter-ictal tensors. Thus, the dataset is divided into *five folds*. One fold is picked for testing of the CNN and the other four folds are left for training. This process, of choosing one fold for testing and the rest for training, is repeated five times (five-fold cross-validation). This process results in five estimates of a performance metric, $metric_1$, …, $metric_5$. The total estimate is computed by averaging these values. Before ictal tensors were discarded, the trained CNN was good at classifying ictal tensors and bad to identify pre-ictal ones. The percentage of ictal observations was much larger than the percentage of pre-ictal ones. This was the motivation for the generation of a balanced training set by discarding ictal observations.

4.7. Performance assessment metrics

During testing of the seizure predicting system, if a pre-ictal tensor is correctly identified then this case is a *TRUE POSITIVE* (TP); otherwise, if it is misclassified this case corresponds to a *FALSE NEGATIVE* (FN). Inter-ictal tensors, correctly classified, correspond to *TRUE NEGATIVES* (TN), while misclassified inter-ictal tensors correspond to *FALSE POSITIVES* (FP). To evaluate the performance of the proposed method, *sensitivity*, *specificity*, *positive predictive value*, *negative predictive value*, *accuracy*, *Matthew Correlation Coefficient*, and F_1 *score* are used as figures of merit. *Sensitivity* (also known as *recall*) or *True Positive Rate* (TPR) is the probability that the outcome of predicting epileptic seizures is positive given that the patient is going to present epileptic seizures, $TPR = \frac{TP}{TP+FN}$. *Specificity* (also known as *selectivity*) or *True Negative Rate* (TNR) is defined as the probability that the outcome of seizure prediction is negative given that the patient is not going to present seizures according to $TNR = \frac{TN}{TN+FP}$.*Precision* or *Positive Predictive Value* (PPV) is the percentage of correctly detected seizures, $PPV = \frac{TP}{TP+FP}$. *Negative Predictive Value* (NPV) is the percentage of correctly detected normal (non-seizure) activity, $NPV = \frac{TN}{TN+FN}$. *Accuracy* is the percentage of detected events that are real according to $Accuracy = \frac{TP+TN}{TP+FP+TN+FN}$. The *Matthews Correlation Coefficient* (MCC) is a correlation coefficient between the observed and predicted binary classifications. It returns a value between -1 and $+1$, $MCC = \frac{TP \times TN - FP \times FN}{\sqrt{(TP+FP)(TP+FN)(TN+FP)(TN+FN)}}$. The F_1 *score* is the harmonic mean of precision and recall, $F_1 = 2\frac{PPV \times TPR}{PPV+TPR}$. The *Receiver Operating Characteristic* (ROC) curve is the plot of the true positive rate (TPR) against the false positive rate (FPR) in a binary classifier when its threshold is varied.

5. Results

Fig. 4 shows the ictal, inter-ictal and pre-ictal states within the recordings of (1) a single channel of EEG (specified in micro-volts [μV]); (2) three states within HbO and HbR recordings (specified in changes in hemoglobin concentration [C]). Finally, parts B), C), D), E) and F) show the specific placement of hundreds of optodes on five different patients, where blue lines represent sources and red lines represent detectors at different optode positions.

For each patient, experiments were conducted over three different combinations of HbO and HbR values: (1) two-dimensional tensors extracted from HbO measurements, (2) two-dimensional tensors extracted from HbR measurements, and (3) three-dimensional tensors extracted from fNIRS (HbO and HbR measurements). Table 2 shows epileptic prediction performance for each patient with three different combinations per patient (HbO, HbR, fNIRS). Seizure prediction rates apply within a two- or five-minute pre-ictal interval before ictal.

Table 2
Performance metrics of the seizure predictor for patients 16, 22 and 26 for three different combinations: HbO, HbR, and fNIRS (HbO + HbR).

Patient	Performance Metric	HbO	HbR	fNIRS
16	TPR	100	100	100
	TNR	100	100	100
	PPV	100	100	100
	NPV	100	100	100
	ACC	100	100	100
	MCC	99.99	99.99	100
	F1	100	100	100
22	TPR	100	98.25	100
	TNR	99.99	99.74	100
	PPV	99.99	99.73	100
	NPV	100	98.28	100
	ACC	99.99	98.99	100
	MCC	100	98.00	99.99
	F_1	99.99	98.99	100
26	TPR	100	100	100
	TNR	100	100	100
	PPV	99.99	100	100
	NPV	100	100	100
	ACC	99.99	100	100
	MCC	99.98	99.98	100
	F_1	99.99	100	100
Patient	Performance Metric	HbO	HbR	fNIRS
38	TPR	95.24	97.04	97.14
	TNR	98.57	99.33	99.52
	PPV	98.52	99.32	99.51
	NPV	95.39	97.11	97.21
	ACC	96.90	98.18	98.33
	MCC	93.39	96.41	97.00
	F_1	96.85	98.17	98.31
47	TPR	100	100	100
	TNR	100	99.99	100
	PPV	100	100	100
	NPV	100	99.99	100
	ACC	100	100	100
	MCC	99.99	99.98	100
	F_1	99.99	99.99	100

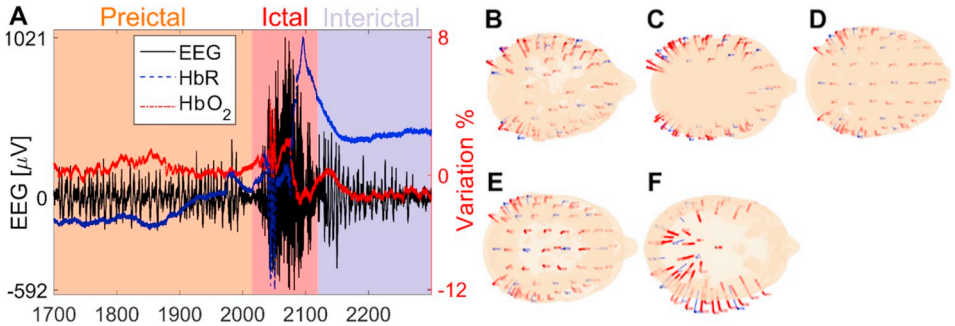

Fig. 4. Illustration of different states (Panel A) in one EEG channel (black curve), one HbO channel (blue curve), and one HbR channel (red curve), along with the position of optodes for the recording of fNIRS signals from five different patients (Panels B, C, D, E, F).

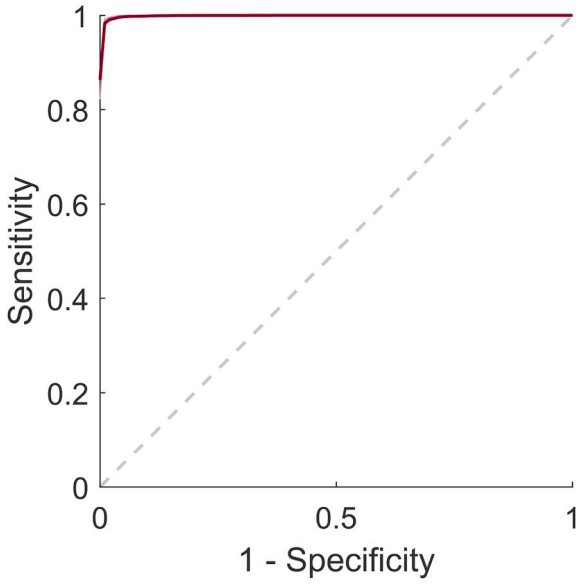

Fig. 5. Average ROC curve for five patients (HbO measurements).

Table 3
Accuracy of a seizure predicting system considering EEG signals and two classical classifiers.

Patient	MLP	SVM
16	0.8152	0.955
22	0.7843	0.952
26	0.5830	0.900
38	0.8275	0.971
47	0.7881	0.960

Plot, of the average ROC curve for five classifiers (patients) and HbO measurements, is shown in Fig. 5.

For each patient, EEG and fNIRS recordings were acquired simultaneously to compare seizure prediction based on fNIRS with that based on EEG. Because of the small number of EEG channels, these channel values were stored in feature vectors (not in tensors) and two standard classifiers were applied for each patient, a Multi-Layer Perceptron (MLP) and a Support Vector Machine (SVM). Table 3 shows the accuracy of epileptic prediction based on EEG signals and two classifiers. The MLP consists of one hidden layer with ten neurons and the number of input nodes is equal to the number of EEG channels. The SVM uses a Gaussian kernel function and the number of input nodes equals the number of EEG channels.

For each patient and each combination of measurements (HbO, HbR), a selection of a CNN architecture is made after training and testing separate architectures for each possible combination of parameters (model selection): number of kernels (1, 2 and 3) at each convolutional layer and different kernel receptive fields (3×3, 5×5 and 7×7). Final parameter values (kernel dimensions and number of kernels at each convolutional layer) are presented in Table 4. The total number of kernel coefficients is computed according to *number of kernel coefficients* $= \sum_{\ell=1}^{3}$ (*number of kernels at layer* $\ell \times$ *kernel dimensions*), which is 90 for classification of three-dimensional tensors and 72 for the case of two-dimensional tensors.

For each patient, the input tensor height (number of rows) is different since this parameter corresponds to the number of channels, which were used to extract fNIRS signals. The second column of Table 1 shows the number of channels for each patient. Fig. 6 shows the implementation of the CNN architecture for patient 22, where the input tensor contains both measurements, HbO and HbR (three-dimensional format). By using the notation, introduced in Section 3, the input data tensor dimensions for patient 22 are $H_D^0 = 133$ (channels), $W_D^0 = 125$ (time positions) and $D_D^0 = 2$ (measurements per channel), where a super-index value of zero refers to the fact that this tensor is fed to layer 1. Tensor dimensions are reduced at subsequent convolutional layers

Table 4
Parameters at each layer of a convolutional neural network.

	Number of kernels	kernel dimensions	Pooling window dimensions
first conv. layer	2	$3 \times 3 \times 2$ for *3-D tensors* or $3 \times 3 \times 1$ for *2-D tensors*	3×3
second conv. layer	2	$3 \times 3 \times 2$	3×3
third conv. layer	1	$3 \times 3 \times 2$	3×3

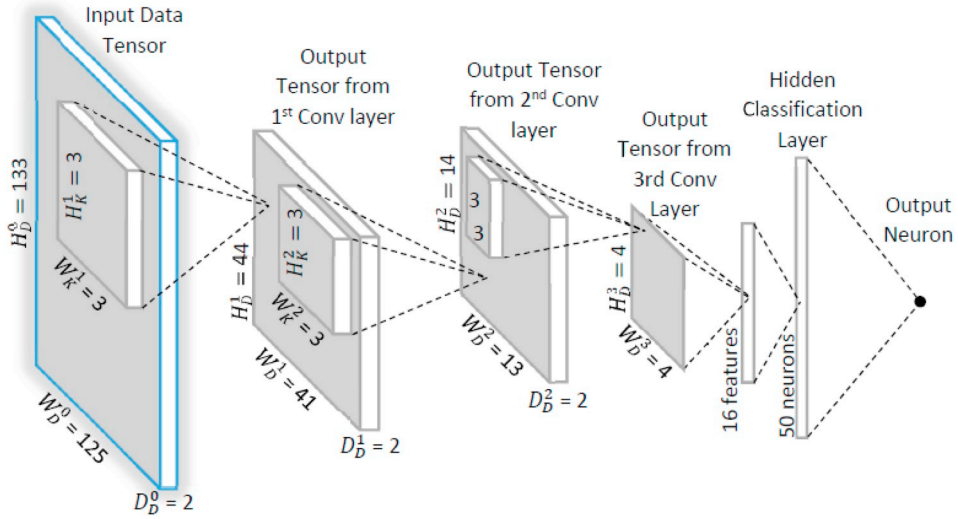

Fig. 6. CNN architecture for tensors with HbO and HbR measurements extracted from patient 22.

Table 5
Data dimensions at the CNN input and at the output of each convolutional and classification layer.

Patient	Input Tensor	1st layer output tensor	2nd layer output tensor	3rd layer output tensor	Input Vector to Classifier
16	$H_D^0 = 146\ W_D^0 = 125\ D_D^0 = 1$ or 2	$H_D^1 = 48\ W_D^1 = 41\ D_D^1 = 2$	$H_D^2 = 16\ W_D^2 = 13\ D_D^2 = 2$	$H_D^3 = 5\ W_D^3 = 4\ D_D^3 = 1$	20 features
22	$H_D^0 = 133\ W_D^0 = 125\ D_D^0 = 1$ or 2	$H_D^1 = 44\ W_D^1 = 41\ D_D^1 = 2$	$H_D^2 = 14\ W_D^2 = 13\ D_D^2 = 2$	$H_D^3 = 4\ W_D^3 = 4\ D_D^3 = 1$	16 features
26	$H_D^0 = 104\ W_D^0 = 125\ D_D^0 = 1$ or 2	$H_D^1 = 34\ W_D^1 = 41\ D_D^1 = 2$	$H_D^2 = 11\ W_D^2 = 13\ D_D^2 = 2$	$H_D^3 = 3\ W_D^3 = 4\ D_D^3 = 1$	12 features
38	$H_D^0 = 138\ W_D^0 = 125\ D_D^0 = 1$ or 2	$H_D^1 = 46\ W_D^1 = 41\ D_D^1 = 2$	$H_D^2 = 15\ W_D^2 = 13\ D_D^2 = 2$	$H_D^3 = 5\ W_D^3 = 4\ D_D^3 = 1$	20 features
47	$H_D^0 = 135\ W_D^0 = 125\ D_D^0 = 1$ or 2	$H_D^1 = 45\ W_D^1 = 41\ D_D^1 = 2$	$H_D^2 = 15\ W_D^2 = 13\ D_D^2 = 2$	$H_D^3 = 5\ W_D^3 = 4\ D_D^3 = 1$	20 features

because of pooling. At the first convolutional layer, the output data tensor dimensions are $H_D^1 = 44$, $W_D^1 = 41$ and $D_D^1 = 2$, where dimensionality reduction is achieved through the use of a 3×3 pooling window, according to $W_D^1 \times H_D^1 = \frac{W_D^0}{3} \times \frac{H_D^0}{3}$. At each layer ℓ, the kernel receptive field is $W_K^l \times H_K^l = 3 \times 3$ as it is shown in Table 4. The dimensions for the output data tensor at the third layer are $H_D^3 = 4$, $W_D^3 = 4$ and $D_D^3 = 1$; and this tensor is stretched out into a 16-feature vector, which is fed to a 50-neuron hidden classification layer. The output classification layer consists of one neuron, which assigns one of two classes (pre-ictal or inter-ictal) to the input data tensor.

Table 5 shows the dimensions of a tensor flowing over three convolutional layers for each patient. At each convolutional layer, output tensor dimensions are reduced through pooling. According to Section 3, three operations are sequentially executed at each convolutional layer, convolution, activation, pooling. *Zero padding* is used at tensor borders during convolution. *Activation* normalizes tensor values so that they lie in the range $(-1, 1)$ by using the hyperbolic tangent function. *Pooling* does not affect previous normalized values since the pooling operation performs an average on normalized values.

Besides the number of kernels and kernel dimensions, there are additional CNN architecture parameters such as *number of convolutional layers*, *number of classification layers*, *number of neurons per classification layer*. The CNN architecture parameters, for each patient, are shown in Table 6. The number of convolutional layers was defined according to the input tensor dimensions and pooling window dimensions. At each layer, the optimal kernel size is 3×3, which allows an architecture with three convolutional layers. The number of synaptic weights at the classification layers is computed according to *number of weights = number of entries in input feature vector* $\times$ 50 *hidden neurons* + 50 *wt at the output neuron* + 51 *bias*.

The size of the set of observations, which is used for training and testing a CNN, depends on the number of seizures during recording sessions, pre-ictal window elapsed time, and sampling rate. For the case of patients 16 and 26, who presented one single seizure during recording sessions, the *number of ictal samples* is *seizures* $\times$ *pre-ictal window* $\times$ *sampling rate* = 1 *seizure* $\times$ 300 *s* $\times$ 500 *samples per second* = 150,000 *pre-ictal samples*. Since the number of pre-ictal observations should match the number of inter-ictal samples to have a two-class balanced set, the final set contains 300,000 observations. This set size is suitable for training and validating a CNN. To avoid overfitting of a CNN, two steps were followed during training. (1) Instead of using 10-fold cross-validation, we used 5-fold cross-validation, where 80% of the observations (240,000 for patients with only one seizure) are used for training and 20% for testing (60,000 observations). (2) During CNN learning, half of the testing set (10%) is used for monitoring of the mean square error (MSE) while the other half (10%) was used for the computation of performance metrics. The training MSE and testing MSE decreased monotonically without a U-shape in the testing MSE before all the epochs were completed.

Table 6
Parameters of convolutional neural networks for five patients.

Patient	Input tensor width	Input tensor height	number of conv. layers	number of class. layers	neurons at hidden class. layer	neurons at output class. layer
16		146				
22		133				
26	125	104	3	2	50	1
37		138				
48		135				

6. Discussion

According to Table 2, epileptic seizure prediction, based on the application of CNN to fNIRS recordings, is effective since performance metrics reach values above 95%. The performance of seizure prediction, when HbO and HbR are jointly used, is higher than that obtained by using only single reading, HbO or HbR. The HbO-HbR (fNIRS) integration allows higher prediction rates since this combination allows convolutional layers to extract more relevant features, which provides spatial and temporal interaction. Both measurements are extracted at the same scalp position. According to Tables 2 and 3, the seizure predicting system, based on fNIRS and CNN, yields results that are superior to those of methods based on EEG and classical classifiers. Thus, fNIRS, a relatively new technique, might be used to predict seizures. Seizure prediction is effectively achieved within a five- or two-minute window (pre-ictal segment), which occurs right before seizure onset. Thus, there is enough time to take precautions before a seizure occurs. The number of kernel coefficients at convolutional layers (72 or 90) and the number of coefficient weights are very high. The implication of having a large number of parameters and high-dimensional input tensors is a high computational time while training a CNN. Training sets contain more than 300,000 observations, a size that is suitable for the training and validation of a CNN. The computational time during real-time tensor classification is low since the number of CNN layers is low (three layers). Given that the data tensor width was chosen as $W = 125$, the elapsed time of a tensor is $\frac{W \text{ samples per tensor}}{500Hz} = 0.25\,s$. Although a direct comparison of our method with current approaches is difficult, due to the use of different datasets, some results on the detection and prediction of epileptic seizures are shown in Table 7. The purpose of Table 7 is to show different methodologies and corresponding results, proposed by the scientific community, working on epileptic seizure prediction with datasets, which do not use the fNIRS modality.

The proposed method solves a binary classification problem that involves separating inter-ictal activity from pre-ictal activity. The identification of pre-ictal observations allows the prediction of epileptic seizures. Different methodologies, in Table 7, solve the problem through a binary classification of an observation, which is identified as inter-ictal (also labeled as normal or non-seizure activity) or ictal (also labeled as a seizure) [34–39,41]. Seizures are detected when they are occurring so that precautions cannot be taken before the occurrence of an epileptic seizure. One method identifies four different classes inter-ictal, pre-ictal, ictal and post-ictal [40]. The proposed method detects seizure activity within time segments of 0.25 s. Published works, in the literature, consider the detection of seizures by using signal segments of duration longer than 2 s with 1-s overlap between segments [34], 2.5 s with an overlap of 0.5 s [41], 4–12 s [37], 4 s [38], 5 s [40], 8 s with 4-s overlap [35], 16 s [39], 23.6 s [36,39]. Some of these works incorporate

Table 7
Some methods for seizure detection.

Author, Year	Detection Algorithm	Results
Petersen et al., 2011 [34]	Wavelet transform, SVM classification, one single EEG channel	Sensitivity of 99.1%
Temko et al., 2011 [35]	Fast Fourier Transform for feature extraction, SVM to detect neonatal seizures from EEG	Sensitivity of 89%
Acharya et al., 2011 [36]	Spectra-based feature extraction, SVM classifiers from EEG	Accuracy of 98.5%
Kharbouch et al., 2011 [37]	Multistep feature extraction, SVM classifiers from EEG	97% of the seizures detected
Liu et al., 2012 [38]	Wavelet decomposition feature extraction, SVM classification from EEG	Sensitivity of 94.5%
Xie et al., 2012 [39]	Feature extraction by wavelet sparse fuctional linear model, 1-NN classification from 6 EEG channels	Accuracy from 99% to 100%
Direito et al., 2012 [40]	Markov modeling classification from EEG	Accuracy of 89.3%
Rabbi et al., 2012 [41]	Fuzzy algorithms for feature extraction, classification from EEG/GTCS, SPS, CPS	Sensitivity of 95.8%
Beniczky et al., 2013 [42]	Time-domain and frequency-domain algorithms with a 3-D accelerometer worn on the wrist	Sensitivity of 91%

a temporal constraint where at least some consecutive time intervals must be classified as containing seizure activity before a seizure is detected (not predicted) [34,37]. One method was based on segments of different time lengths since different datasets were employed [39]. We are using fNIRS-EEG recordings with a total duration of 58 h from 49 epileptic patients where 357.69 min (6 h) correspond to patients who showed seizures. This dataset contains a total of 22 detectable seizures from five epileptic patients, where five classifiers are trained. One advantage of the proposed method is that the observation segment is of very short duration (when compared with other methods), which allows for a very large number of observations. In the set of experiments, the smallest set to train and test a classifier contains 300,000 pre-ictal and ictal observations. To the best of our knowledge, there are not public fNIRS datasets, obtained from epileptic patients; however, published works are based on public EEG datasets with different total recording times: 708 min (111 detectable seizures from children) [34], 267.9 h from 17 newborns [35], 875 h (67 seizures) from 10 patients [37], 4808 min from 21 patients [38], 9 h from 5 patients [39], 497.3 h (30 seizures) from 10 patients [40], 112.45 h (56 seizures) from 21 patients [41]. Although some public EEG datasets are characterized by a larger recording time than that of the fNIRS dataset that we used, the number of training observations is smaller: 705 8-s ictal segments [35], 2359 4-s ictal segments and 69,753 4-s inter-ictal segments [38], 5400 inter-ictal 16-s segments and 240 ictal segments [39], 100 ictal segments and 100 inter-ictal 23.6-s segments [36,39]. Other seizure predictive methods usually use two-layer classical classifiers, such as those in Table 7; however, these methods require previous processing time for feature extraction from signals at multiple time positions.

7. Conclusions

The problem of predicting epileptic seizures, using deep learning and fNIRS recordings, was studied. It is shown that the application of CNN to fNIRS data is suitable given the nature of fNIRS, which can be modeled as two- or three-dimensional tensors of high dimensionality. Evidence of the effectiveness of the proposed method is obtained through assessment of different performance metrics such as *accuracy* ranging between 96.9% and 100%, *sensitivity* between 95.24% and 100%, and *specificity* between 98.57% and 100%. Moreover, it is demonstrated that fNIRS recordings outperform EEG recordings when they are used for epileptic seizure prediction. An aspect to consider in the implementation of the proposed method is that a learning machine is trained for each patient since the number of channels per patient was different. The motivation, of applying convolution to fNIRS data, is that the spatial correlation between HbO and HbR (both values are measured at the same scalp position) is maintained within a three-dimensional tensor. A disadvantage of the application of CNNs to fNIRS recordings is the high computational time during thirty epochs of CNN training in a MATLAB implementation. The most important aspect of obtaining these results is the combination of fNIRS signals with the particular CNN algorithm. This project is one of the first investigations based on the fNIRS modality and deep learning to address the problem of epileptic seizure prediction.

Acknowledgement

This work was supported in part by a Mexico-Quebec Mobility program (project No. 265578). Data recordings were obtained from Hôpital Notre-Dame du Centre Hospitalier de l'Université de Montréal. Edgar Guevara acknowledges support from “Cátedras CONACYT” project 528.

References

[1] N. Moghim, D.W. Corne, Predicting epileptic seizures in advance, PLoS One 9 (6) (2014) e99334, , https://doi.org/10.1371/journal.pone.0099334.
[2] S. Ramgopal, S. Thome-Souza, M. Jackson, N.E. Kadish, I. Snchez-Fernndez, J. Klehm, W. Bosl, C. Reinsberger, S. Schachter, T. Loddenkemper, Seizure detection, seizure prediction, and closed-loop warning systems in epilepsy, Epilepsy Behav. 37 (2014) 118–173, https://doi.org/10.1016/j.yebeh.2014.06.023.
[3] D.K. Binder, S.R. Haut, Toward new paradigms of seizure detection, Epilepsy Behav. 26 (3) (2013) 247252, https://doi.org/10.1016/j.yebeh.2012.10.027.
[4] E. Guevara, K. Nguyen, K. Peng, P. Pouliot, Epileptic seizure detection in fNIRS signals using a supervised classifier, Proc. fNIRS (2014).
[5] H. Obrig, NIRS in clinical neurology a promising tool? Neuroimage 85 (1) (2014) 535546, https://doi.org/10.1016/j.neuroimage.2013.03.045.
[6] P. Pouliot, J. Tremblay, M. Robert, P. Vannasing, F. Lepore, M. Lassonde, M. Sawan, D.K. Nguyen, F. Lesage, Nonlinear hemodynamic responses in human epilepsy: a multimodal analysis with fNIRS-EEG and fMRI-EEG, J. Neurosci. Methods 204 (2) (2012) 326340, https://doi.org/10.1016/j.jneumeth.2011.11.016.
[7] J. Ingram, C. Zhang, J.R. Cressman, A. Hazra, Y. Wei, Y.E. Koo, J. iburkus, R. Kopelman, J. Xu, S.J. Schiff, Oxygen and seizure dynamics: I. experiments, J. Neurophysiol. 112 (2) (2014) 205212, https://doi.org/10.1152/jn.00540.2013.
[8] C.S. Hawco, A.P. Bagshaw, Y. Lu, F. Dubeau, J. Gotman, BOLD changes occur prior to epileptic spikes seen on scalp EEG, Neuroimage 35 (4) (2007) 1450–1458, https://doi.org/10.1016/j.neuroimage.2006.12.042.
[9] M. Zhao, J. Nguyen, H. Ma, N. Nishimura, C.B. Schaffer, T.H. Schwartz, Preictal and ictal neurovascular and metabolic coupling surrounding a seizure focus, J. Neurosci. 31 (37) (2011) 13292–13300, https://doi.org/10.1523/JNEUROSCI.2597-11.2011 http://www.ncbi.nlm.nih.gov/pubmed/21917812.
[10] P. Camfield, C. Camfield, Idiopathic generalized epilepsy with generalized tonic-clonic seizures (IGE-GTC): a population-based cohort with more than 20 year follow up for medical and social outcome, Epilepsy Behav. 18 (1–2) (2010) 6163, https://doi.org/10.1016/j.yebeh.2010.02.014.
[11] P. Gmez-Gil, E. Jurez-Guerra, V. Alarcn-Aquino, J.M. Ramrez-Corts, J. Rangel-Magdaleno, Identification of epilepsy seizures using multi-resolution analysis and artificial neural networks, Recent Adv. Hybrid Approaches Des. Intell. Syst. 547 (2014) 337–351, https://doi.org/10.1007/978-3-319-05170-3_23.
[12] A. T. Tzallas, M. G. Tsipouras, D. G. Tsalikakis, E. C. Karvounis, L. Astrakas, S. Konitsiotis, M. Tzaphlidou, Automated epileptic seizure detection methods: a review study, Epilepsy - Histol. Electroencephalogr. Psychol. Asp. doi:10.5772/31597.
[13] L. Orosco, A.G. Correa, E. Laciar, Review: a survey of performance and techniques for automatic epilepsy detection, J. Med. Biol. Eng. 33 (6) (2013) 526537, https://doi.org/10.5405/jmbe.1463.
[14] F. Mormann, R.G. Andrzejak, C.E. Elger, K. Lehnertz, Seizure prediction: the long and winding road, Brain J. Neurol. 130 (2) (2007) 314333, https://doi.org/10.1093/brain/awl241.
[15] U. Rajendra-Acharya, S. Vinitha-Sree, G. Swapna, R.J. Martis, J.S. Suri, Automated EEG analysis of epilepsy: a review, Knowl. Based Syst. 45 (2013) 147165, https://doi.org/10.1016/j.knosys.2013.02.014.
[16] F. Wallois, A. Patil, C. Hberl, R. Grebe, EEG-NIRS in epilepsy in children and neonates, Neurophysiol. Clin. Clin. Neurophysiol. 40 (5–6) (2010) 281292, https://doi.org/10.1016/j.neucli.2010.08.004.
[17] E. D. Kondylis, T. A. Wozny, W. J. Lipski, A. Popescu, V. J. DeStefino, B. Esmaeili, V. K. Raghu, A. Bagic, R. M. Richardson, Detection of high-frequency oscillations by hybrid depth electrodes in standard clinical intracranial EEG recordings, Front. Neurol. 5 (149). doi:10.3389/fneur.2014.00149.
[18] S. Smith, EEG in the diagnosis, classification, and management of patients with

epilepsy, J. Neurol. Neurosurg. Psychiatry 76 (2) (2005) ii2–ii7, https://doi.org/10.1136/jnnp.2005.069245.
[19] A. Gallagher, M. Lassonde, D. Bastien, P. Vannasing, F. Lesage, C. Grova, A. Bouthillier, L. Carmant, F. Lepore, R. Bland, D.K. Nguyen, Non-invasive pre-surgical investigation of a 10 year-old epileptic boy using simultaneous EEG-NIRS, Seizure J. Br. Epilepsy Assoc. 17 (6) (2008) 576582, https://doi.org/10.1016/j.seizure.2008.01.009.
[20] P. Pinti, C. Aichelburg, F. Lind, S. Power, E. Swingler, A. Merla, A. Hamilton, S. Gilbert, P. Burgess, I. Tachtsidis, Using fiberless, wearable fNIRS to monitor brain activity in real-world cognitive tasks, J. Vis. Exp. 2 (106) (2015) e53336, , https://doi.org/10.3791/53336.
[21] A.M. Chiarelli, F. Zappasodi, F. Di Pompeo, A. Merla, Simultaneous functional near-infrared spectroscopy and electroencephalography for monitoring of human brain activity and oxygenation: a review, Epilepsia 49 (11) (2017) e041411, , https://doi.org/10.1117/1.NPh.4.4.041411.
[22] D.N. Lenkov, A.B. Volnova, A.R.D. Pope, V. Tsytsarev, Advantages and limitations of brain imaging methods in the research of absence epilepsy in humans and animal models, J. Neurosci. Methods 212 (2) (2013) 195–202, https://doi.org/10.1016/j.jneumeth.2012.10.018.
[23] N. Roche-Labarbe, B. Zaaimi, P. Berquin, A. Nehlig, R. Grebe, F. Wallois, NIRS-measured oxy- and deoxyhemoglobin changes associated with EEG spike-and-wave discharges in children, Epilepsia 49 (11) (2008) 18711880, https://doi.org/10.1111/j.1528-1167.2008.01711.x.
[24] A. Machado, O. Marcotte, J.M. Lina, E. Kobayashi, C. Grova, Optimal optode montage on electroencephalography/functional near-infrared spectroscopy caps dedicated to study epileptic discharges, J. Biomed. Opt. 19 (2) (2014) e026010, , https://doi.org/10.1117/1.JBO.19.2.026010.
[25] E. Watanabe, Y. Nagahori, Y. Mayanagi, Focus diagnosis of epilepsy using near-infrared spectroscopy, Epilepsia 43 (9) (2002) 50–55, https://doi.org/10.1046/j.1528-1157.43.s.9.12.x.
[26] J.A. Flores-Castro, K. Peng, D.K. Nguyen, F. Lesage, P. Pouliot, R. Rosas-Romero, E. Guevara, Detecting epileptic seizures in advance using optical and electrical recordings, Proceedings of the 2017 International Conference on Electronics, Communications and Computers (CONIELECOMP), 2017, https://doi.org/10.1109/CONIELECOMP.2017.7891811.
[27] K. Peng, D.K. Nguyen, T. Tayah, P. Vannasing, J. Tremblay, M. Sawan, M. Lassonde, F. Lesage, P. Pouliot, fNIRS-EEG study of focal interictal epileptiform discharges, Epilepsy Res. 108 (3) (2014) 491505, https://doi.org/10.1016/j.eplepsyres.2013.12.011.
[28] D.K. Nguyen, J. Tremblay, P. Pouliot, P. Vannasing, O. Florea, L. Carmant, F. Lepore, M. Sawan, F. Lesage, M. Lassonde, Non-invasive continuous EEG-fNIRS recording of temporal lobe seizures, Epilepsy Res. 99 (1–2) (2012) 112126, https://doi.org/10.1016/j.eplepsyres.2011.10.035.
[29] D.T. Delpy, M. Cope, P. Vand der Zee, S. Arridge, S. Wray, J. Wyatt, Estimation of optical path length through tissue from direct time of flight measurement, Phys. Med. Biol. 33 (12) (1988) 1433–1442.
[30] D.A. Boas, G. Strangman, J.P. Culver, R.D. Hoge, G. Jasdzewski, R.A. Poldrack, B.R. Rosen, J.B. Mandeville, Can the cerebral metabolic rate of oxygen be estimated with near-infrared spectroscopy? Phys. Med. Biol. 48 (15) (2003) 2405–2418.
[31] J.C. Ye, S. Tak, K.E. Jang, J. Jung, J. Janq, Nirs-spm: statistical parametric mapping for near-infrared spectroscopy, Neuroimage 44 (2) (2009) 428447, https://doi.org/10.1016/j.neuroimage.2008.08.036.
[32] T.J. Huppert, S.G. Diamond, M.A. Franceschini, D.A. Boas, HomER: a review of time-series analysis methods for near-infrared spectroscopy of the brain, Appl. Opt. 48 (10) (2009) 280298.
[33] L.D. Iasemidis, Seizure prediction and its applications, Neurosurg. Clin. N. Am. 22 (4) (2011) 489506, https://doi.org/10.1016/j.nec.2011.07.004.
[34] E.B. Petersen, J. Duun-Henriksen, A. Mazzaretto, T.W. Kjaer, C.E. Thomsen, H.B. Sorensen, Generic single-channel detection of absence seizures, Conf. Proc. IEEE Eng. Med. Biol. Soc. 22 (4) (2011) 4820–4823, https://doi.org/10.1109/IEMBS.2011.6091194.
[35] A. Temko, E. Thomas, W. Marnane, G. Lightbody, G. Boylan, EEG-based neonatal seizure detection with support vector machines, Clin. Neurophysiol. (3) (2011) 464473, https://doi.org/10.1016/j.clinph.2010.06.034.
[36] U.R. Acharya, S.V. Sree, J.S. Suri, Automatic detection of epileptic EEG signals using higher order cumulant features, Int. J. Neural Syst. 21 (5) (2011) 464473, https://doi.org/10.1142/S0129065711002912.
[37] A. Kharbouch, A. Shoeb, J. Guttag, S.S. Cash, An Algorithm for Seizure Onset Detection Using Intracranial EEG, Epilepsy Behav, 2011, p. 2935, https://doi.org/10.1016/j.yebeh.2011.08.031.
[38] Y. Liu, W. Zhou, Q. Yuan, S. Chen, Automatic seizure detection using wavelet transform and SVM in long-term intracranial EEG, IEEE Trans. Neural Syst. Rehabil. Eng. 20 (6) (2012) 749755, https://doi.org/10.1109/TNSRE.2012.2206054.
[39] S. Xie, S. Krishnan, Wavelet-based sparse functional linear model with applications to EEGs seizure detection and epilepsy diagnosis, Med. Biol. Eng. Comput. 51 (1–2) (2012) 49–60, https://doi.org/10.1007/s11517-012-0967-8.
[40] B. Direito, C. Teixeira, B. Ribeiro, M. Castelo-Branco, F. Sales, A. Dourado, Modeling epileptic brain states using EEG spectral analysis and topographic mapping, J. Neurosci. Methods 210 (2) (2012) 220229, https://doi.org/10.1016/j.jneumeth.2012.07.006.
[41] A.F. Rabbi, R. Fazel-Rezai, A fuzzy logic system for seizure onset detection in intracranial EEG, Comput. Intell. Neurosci. 2012 (2012) 1–12, https://doi.org/10.1155/2012/705140.
[42] S. Beniczky, T. Polster, T.W. Kjaer, H. Hjalgrim, Detection of generalized tonicclonic seizures by a wireless wrist accelerometer: a prospective, multicenter study, Epilepsia 54 (4) (2013) 5861, https://doi.org/10.1111/epi.12120.